Research Article Vol. 30, No. 6 / 14 Mar 2022 / Optics Express 9674
Optics EXPRESS

Spectro-temporal behavior of dye-based solid-state random lasers under picosecond pumping regime

I. IPARRAGUIRRE,[1,*] J. AZKARGORTA,[1] S. GARCÍA-REVILLA,[1] J. FERNÁNDEZ,[2] AND R. BALDA[1,2,3]

[1] Universidad del País Vasco UPV/EHU, Dpto. de Física Aplicada, Escuela de Ingeniería de Bilbao, Plaza Ingeniero Torres Quevedo 1, 48013 Bilbao, Spain
[2] Donostia International Physics Center DIPC, 20018 San Sebastián, Spain
[3] Materials Physics Center CSIC-UPV/EHU, 20018 San Sebastián, Spain
[*] jon.azkargorta@ehu.es

Abstract: In this work, the spectral and temporal properties of the random laser emission from dye-doped solid state powders are investigated in picosecond pumping regime. Ultrafast time-resolved spectroscopy achieved with a streak-camera has been used to perform a detailed study of the temporal evolution of the spectrum of their single pulses. Under conditions of low population inversion density, it is observed that the detected radiation occurs as isolated peaks with a very narrow spectro-temporally spread ($\Delta\omega\Delta t \cong 1$). This behavior remains under conditions of high population inversion density, suggesting that the underlying physical mechanism that produces the emission is the same whatever the pumping conditions. Measurements carried out by varying the numerical aperture of the detection system show that each detected peak within a single pulse is associated with a photon pack emitted in a random direction and wavelength. The relationship between the distribution of paths lengths done by photons inside the active medium, and the gain explains the observed behavior.

1. Introduction

Random lasers (RLs) are very interesting radiation emitters, with applications such as lithography, high definition speckle free imaging, holographic laser displays, optical sensors for medical and other applications [1–6]. Materials with different properties have been tested as source of RL radiation: polymers, crystal powders, colloidal dye solutions, biological samples and others, showing a very varied behavior in terms of energy efficiencies, emission spectra and ranges of pulse time [7–13]. In particular, solid-state dye RLs have attracted attention because of advantages in comparison with liquid dye lasers for some applications. Research has been done on efficiency and photo-stability, material hosts for good dispersion of dyes or energetic behavior [14–18].

One of the most extensively studied issues in dye RLs is the spectral behavior [16,19–30]. Our interest is focused on the temporal behavior of the spectrum within each emitted pulse. There are works that deal with this question in different materials and hosts [24,27–30]. Some propose the existence of relaxation oscillations in the emission, without having knowledge of the temporal profile of the pumping pulse, which could lead to inappropriate interpretations, also in inorganic powders [27,31–34], since the pumping can have a time profile strongly affected by the beating of longitudinal modes or other effects [35]. The temporal resolution limit determines the nature of the observed results and in ns pumping regime, it has been observed that the RL emission follows more or less faithfully, the temporal profile of the pumping pulse [22,26], although it depends on how it is measured [36].

#451017 https://doi.org/10.1364/OE.451017
Journal © 2022 Received 19 Dec 2021; revised 9 Feb 2022; accepted 9 Feb 2022; published 9 Mar 2022

Optics EXPRESS

We are going to investigate this question under picosecond pumping regime, in which, if sufficient resolution is available, effects that do not appear in slower regimes could be observed. The work will be done using a Solid-State Dye Random Laser (SSDRL) as active medium.

In terms of energies, the behavior of SSDRL in ps pumping regime is quite similar to the Neodymium doped powders in ns pumping regime, because in both cases the pumping time is very short compared to their respective spontaneous decay time [18]. In terms of time dynamics, measurements in Nd^{3+} doped inorganic powders show that the detected RL intensity has a different temporal profile depending on the size of the detection area [36]. If the magnitude $\lambda L/\Phi^2$ is much greater than unity, being λ the wavelength, L the emitter-detector distance and Φ the size of the detector, the detector can be considered a point detector as all points in its area receive the same signal. Then, sub-ns fluctuations can be observed if the temporal resolution of the measurement system is fast enough. In the opposite case, the resulting profile is quite similar to that of the corresponding pump pulse [22,26]. Analogous results are obtained in SSDRLs in ns pumping regime, and we can say that in general the RL emission follows the pumping pulse quite closely above threshold [37].

Regarding the threshold, it must be said that specially in dyes, it is not experimentally very well defined. If we measure the intensity emitted, below a given level of pump energy the measurement will be confused with noise. Above that level, under standard conditions, a concentration of peaks begins to be observed by the streak-camera during the pumping time, which agrees with the observed spectral narrowing around threshold. In our opinion it is not possible to give a precise value of the threshold energy, because ultimately it depends on what and how exactly is being measured, and even so, has a certain component of subjectivity. In our case, an uncertainty of approximately ±5% is accepted, and with the pump beam size used over our sample a value of 40μJ is achieved.

Our aim is to investigate the temporal dynamics of the spectral structure of the emission of SSDRL in ps pumping regime with high temporal resolution. It should be noted that this type of study cannot be carried out in Nd^{3+} doped powders due to their narrow emission bands. Consequently, the spectral intensity of a single pulse (not the average) will be recorded with a temporal resolution better than ps and spectral resolution better than nm, being possible to obtain the intensity at any wavelength and the spectrum at any time for each detected pulse. On the other hand, the detection area in our measurement set-up will be small enough to be considered punctual in the sense cited above, which can be very important when interpreting the results. The observed behavior will be explained in terms of the relationship between the distribution of paths of different lengths done by photons inside the active medium and the gain in these paths.

2. Measurement set-up

The active medium of SSDRL samples are Rhodamine B-doped di-ureasil powders [30], with concentrations close to 5×10^{18} molecules/cm^3. Their diffuse absorbance is somewhat greater than 50%, their inelastic length about 20 micron and their transport length about 30 micron [38–37] with a volume filling factor of 55%.

The experimental system is described in Fig. 1. Samples are excited with a doubled Nd:YAG laser (EKSPLA PL2251B) delivering 30 ps pulses at 532 nm wavelength. The pumping energy is attenuated with a half-wave plate combined with a polarizer and measured with an energy meter. The pump beam can be concentrated to the desired diameter by means of a movable lens L1. The radiation emitted by the SSDRL is collimated by a lens L2 of 50 mm focal length and a diameter of 25 mm and projected by the lens L3, so that the image of the emitting surface can be focused on the center of the entrance slit of the imaging spectrograph (Chromex). Reflected pumping is removed by a long-pass filter F, sometimes only partially, in order to have the pump pulse reference.

Optics EXPRESS

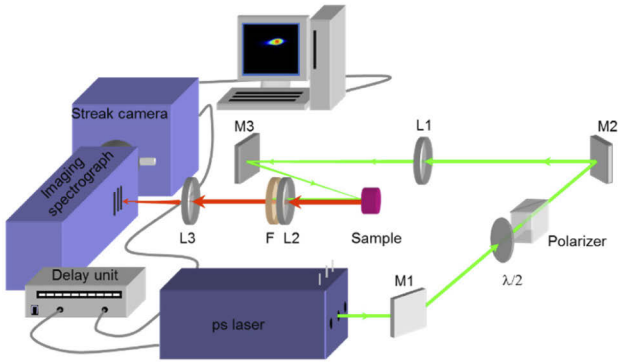

Fig. 1. Scheme of the experimental set-up. M1, M2 and M3 are mirrors, L1, L2 and L3 are lenses and F is a long-pass filter.

The slit width employed at the entrance of the spectrograph is 20 micron, and the measured FWHM for a He-Ne laser using this width is 0.3 nm, which we consider the spectral apparatus function of the detection system. The spectrograph is connected to a streak camera (C5680 Hamamatsu) so with appropriate optics, the spectrum of radiation on its entrance slit is projected onto the entrance slit of the streak camera, previous to the photocathode. This slit is perpendicular to that of the spectrograph and its width is 10 microns. Therefore, we can consider that the signal captured by the spectrograph-streak camera system is the one that reaches the center of the entrance slit, and its size is about ten microns, which is small enough to be considered a point in the sense cited above. We have verified that covering vertically the entire slit except for a very narrow central area, the records were similar and did not decrease in intensity.

The temporal resolution of the streak camera is better than ps in the shortest time range (0.16 ns), and being a system of 512×512 pixels, the temporal width of each pixel is 0.3 ps using this time range and 20 ps/pixel for a time window of 10 ns. The spectral width for each pixel is 0.2 nm using a spectral range of about 100 nm.

3. Results

The measurements have been carried out usually by exciting a large zone of the SSDRL, in particular with a pump spot size of 2 mm in diameter on its surface. Figure 2 shows the streak-camera images of single pulses at three different pumping levels, ((a) above, (b) close and (c) below threshold, which in our experimental conditions is about 40 μJ), recorded in a 160 ps time window, which gives us the best temporal resolution. Figure 3 shows the records of other pulses obtained in the same conditions, but with a 10 ns time window. In each record, the spectral intensity of the detected emission is registered as a function of time. From these experimental results we can infer first, that the spectro-temporal structure does not repeat pulse by pulse and second, each pulse is formed by numerous isolated peaks at apparently random spectral and temporal positions within the spectral range of the emission of the dye as well as within the temporal range of its spontaneous emission. All the streak-camera images were made with the same level of photocathode gain, which can make isolated peaks appear weaker when there is intense lasing and low temporal resolution, as can be seen comparing Figs. 3(a) and 3(c) for example. Nevertheless, the signal-noise ratio level registered for isolated peaks in both figures (after lasing in Fig. 3(a)) is of the same order.

It should be noted that the measurements have been carried out in two different ways. One was in the manner indicated above (Fig. 1), in which only the radiation from a small emitting area of the sample (tens of micron) is captured. The other way was eliminating the L3 lens, thus the

Optics EXPRESS

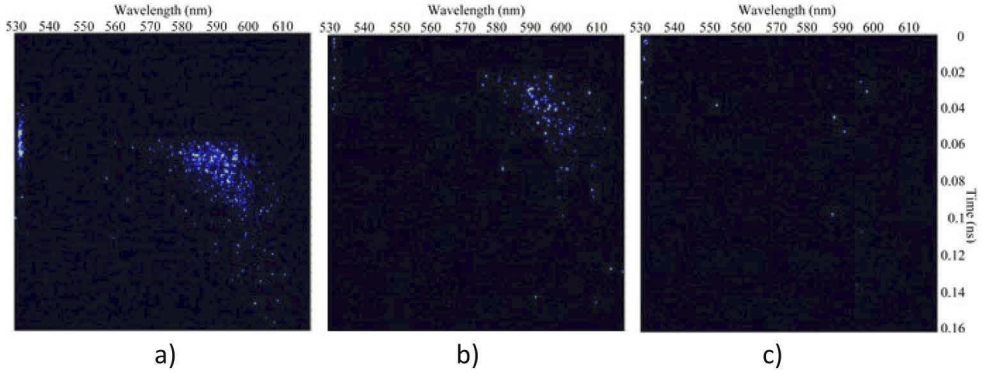

Fig. 2. Streak-camera images of single pulses. Pump beam diameter 2 mm, time window 160 ps, spectral window 530-620 nm. The pump signal is also displayed, using a partial filter. Incident pump energies: a) 100 μJ, b) 60 μJ, c) 20 μJ.

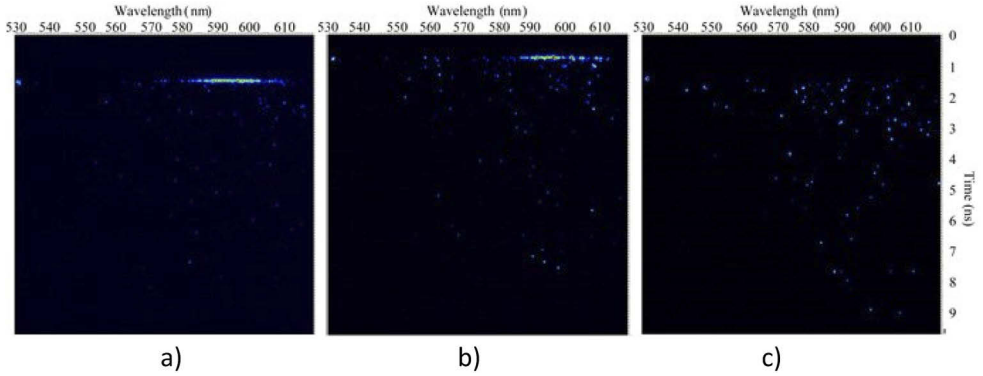

Fig. 3. Record of single pulses in the same conditions as Fig. 2, but in a longer time window (10 ns), pump beam diameter 2 mm, spectral window 530-620 nm. The pump signal is also displayed, using a partial filter. Incident pump energies: a) 100 μJ, b) 60 μJ, c) 20 μJ.

radiation that reaches the center of the entrance slit comes from a much larger area of the emitting surface. It can be said that in one way, many rays from a single point are included and almost unique rays from many points in the other way. The Streak camera images obtained by using both routes result formally indistinguishable, suggesting that the spectro-temporal properties of the emission do not depend on whether the signal collected comes from a very small area of the emitting surface or all of it.

On the other hand, if we use a focused pump beam, giving an emission area of size about 300 micron on the surface of the SSDRL (the emission area is quite larger than the size of the incident beam in these samples [30]), the results are similar. No noticeable changes were found due to an emission area variation.

Each streak-camera image can be integrated spectrally (see example in Fig. 4(a)) and temporally (Fig. 4(b) for the same pulse). Both, the temporally integrated spectrum and the temporally profile extracted spectrally integrating, have quite different shapes pulse to pulse. Clearly above threshold (40μJ in these conditions), the emission pulse has a duration similar to that of the pumping pulse and a spectral width much smaller than that corresponding to the spontaneous emission; in addition, the build-up time is very short. Regarding the observed temporal profile of the reflected pumping pulse, we must bear in mind that its fluctuations have scale times of

Optics EXPRESS

the order of the coherence time of the pumping laser (few ps), so it is rather possible that the temporal profile of the measured reflected intensity depends on the observation point, and that the profile shown in Fig. 4(a) for the pumping intensity does not represent faithfully the real spatially averaged absorbed pump on the sample, which is what really matters.

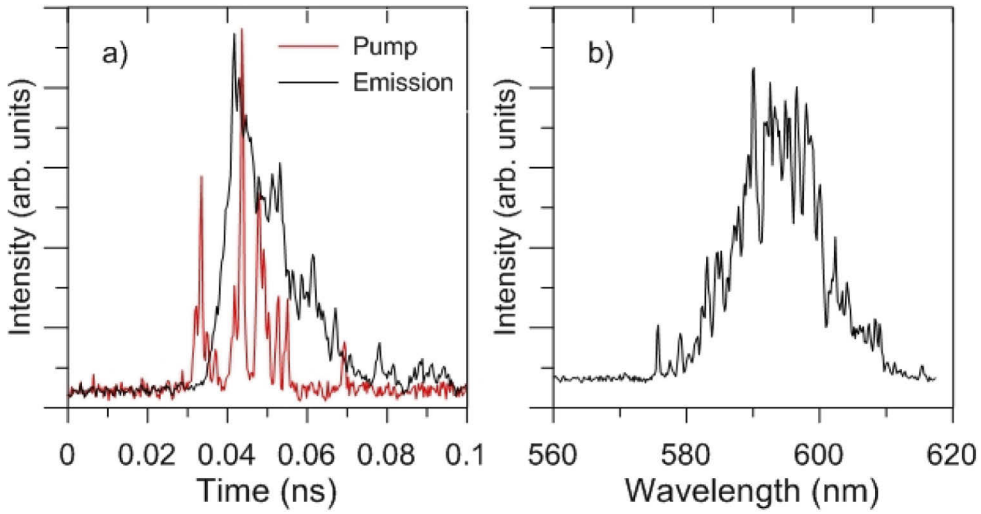

Fig. 4. a) Temporal profile (integrated in spectra) extracted from the streak-camera image of a single pulse SSDRL emission (black) and reflected pumping intensity (red) both obtained from the same single pulse at the same measurement point. The incident pump energy is 100 μJ and the pump beam size is 2 mm in diameter on the SSDRL surface. b) Spectral profile (integrated in time) extracted from the Streak-Camera image from the same pulse.

The average of a high enough number of pulses gives the well-known emission spectrum of the RhB, which narrows with increasing pump energy close to the threshold, and provides a pulse of duration quite similar to the pumping pulse. However, under sub-threshold pumping conditions a pulse lasting about the Rh B spontaneous decay time (some nanoseconds) is obtained.

Let us now focus on the isolated peaks which appear in a single pulse recorded in the 160 ps time window (Fig. 2). We have measured both spectral and temporal FWHM of many of them under different pumping and measurement conditions and we have always obtained very similar results. Their spectral FWHM are in the 0.4-0.6 nm range, whereas their temporal FWHM are in the 0.5-0.8 ps range. It is very noticeable that the product of the width in optical frequency by the temporal width is about 0.3-0.4, which can be actually much less, since we are at the limits of the temporal and spectral resolution of the measurement system. This result suggests that the bunch of photons that form one of these peaks comes from the amplification of a single spontaneous photon.

Above threshold, almost all emission occurs during the pumping pulse (tens of ps). We can explore the apparent correlation in time and wavelength within a single pulse. We show these results in Fig. 5, where one can observe that the temporal profiles extracted at two wavelengths only one nm apart are highly uncorrelated. Likewise, the spectra obtained at two times two ps separated are also highly uncorrelated.

These results suggest that all RL emission of each single pulse from a SSDRL occurs in the form of very short (< 1ps) and spectrally narrow (< 1 nm) peaks, that satisfy that the product of their temporal and spectral widths is the minimum possible. When the population inversion density exceeds the threshold value, the number of emitted peaks is very high, so that they fill

Optics EXPRESS

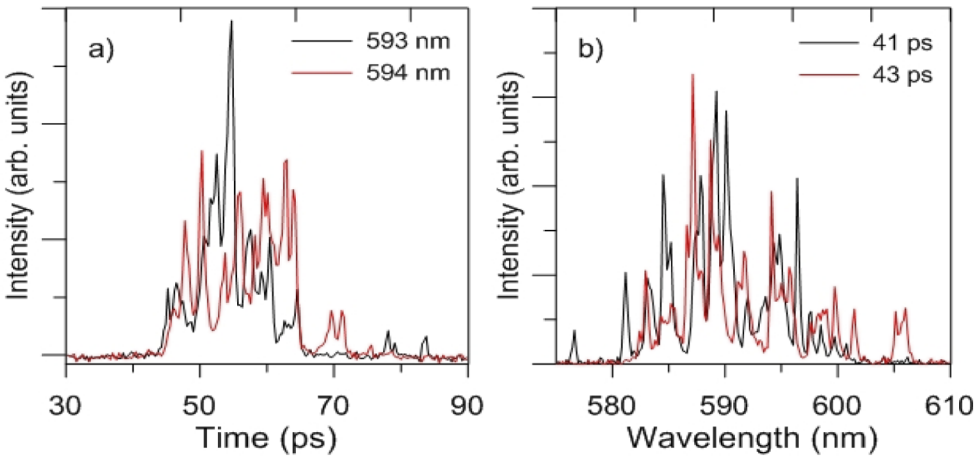

Fig. 5. a) Temporal profiles extracted from the streak-camera image of a SSDRL single pulse by using two vertical pixel lines (about 0.2 nm) at 593 nm wavelength (black) and 594 nm wavelength (red). b) Spectral profiles extracted from the streak-camera image of a SSDRL single pulse by using two horizontal pixel lines (about 0.3 ps) separated 2 ps. The incident pump energy is 100 μJ and the pump beam size is 2 mm in diameter on the SSDRL surface.

the spectral emission band and saturation is reached. In contrast, when the SSDRL is below the threshold, only few isolated peaks are detected, but the emission is done in the same way.

It is important to verify if each one of these peaks is due to radiation emitted multi directionally, or emitted in a determined direction, and it is the whole that gives rise to a multidirectional emission. The way is to observe the effect of varying the numerical aperture at the entrance of the measurement system, which in principle affects the number of rays that reach the measurement area. Usually, the total numerical aperture (NA) employed has been 0.5 (L2: 50 mm focal length and 25 mm in diameter), but we have also carried out measurements limiting the incident rays with a diaphragm in the collimating lens L2 (see Fig. 6). Figure 6(a) shows a pulse obtained without diaphragm, and Fig. 6(b) shows the image obtained under the same pump and gain conditions, but limiting seriously the numerical aperture with an iris of 1 mm in diameter (NA=0.02). As can be observed, very few peaks remain during lasing itself and they practically disappear afterwards.

To make sure of the relationship between the numerical aperture and the number of peaks under the same pumping conditions, we tried the opposite, that is, capture a higher number of rays than usually using a much larger NA system. For this purpose, we have pumped the active medium into an elliptical specular collecting system developed by our group [39], which is able to collect almost all rays (up to 80° respect to the symmetry axis). In this case, the effect is better observed below threshold, because above it, the laser emission obscures a good observation of the rest. Figures 7(a) and 7(b) show results obtained with both numerical apertures. Obviously, the number of rays captured is much greater with the elliptical collecting system.

The set of experimental results described above point to a multiple and omnidirectional emission of photons packs, each one emitted with a determined linear momentum and energy. Therefore, each photon pack is emitted from the SSDRL surface in a defined direction and with a defined wavelength, being its angular width

$$\alpha = \frac{\Delta p_x}{p} = \frac{h/\Delta x}{h/\lambda} = \frac{\lambda}{\Delta x} \approx 10^{-2}\ \text{rad}, \tag{1}$$

Optics EXPRESS

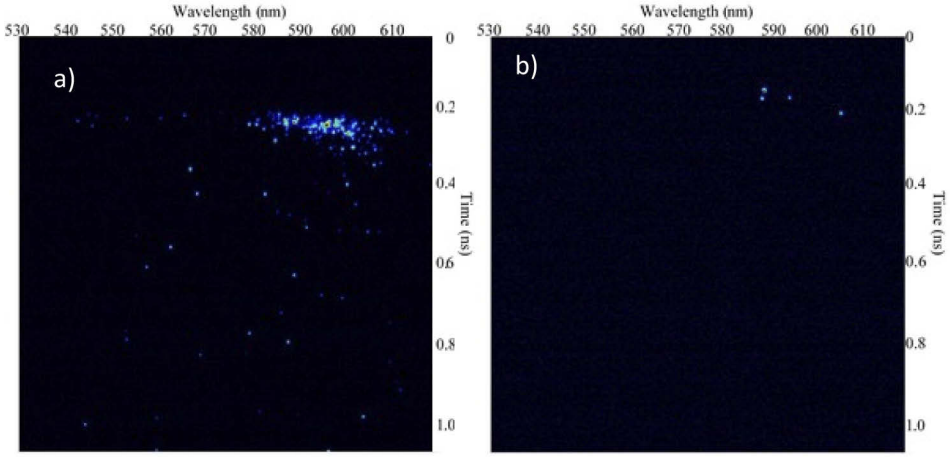

Fig. 6. Streak-Camera images of single pulses obtained: a) Using the usual numerical aperture (NA=0.5) and b) NA = 0.02. In both cases the incident pump energy is 60 μJ and the pump beam size is 2 mm in diameter on the SSDRL surface.

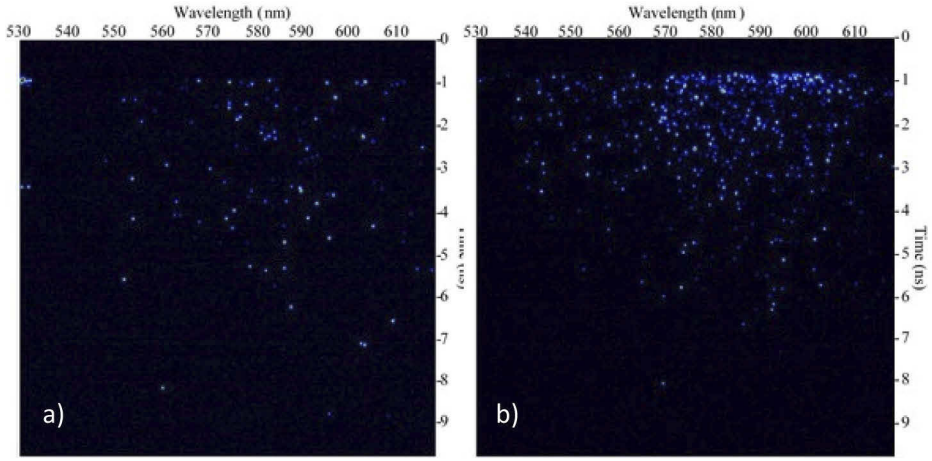

Fig. 7. Streak-Camera images of single pulses obtained a) Using the usual numerical aperture (NA=0.5) and b) Using the collecting system of almost total NA (yield about 75%). In both cases the incident pump energy is 20 μJ and the pump beam size is 2 mm in diameter on the SSDRL surface.

where we have assumed a coherent emission size Δx on the SSDRL surface of the order of the transport length (in the order of ten micron). In fact, this gives a lower angular value than the NA commonly employed (Figs. 6(a) and 7(a)), and it is comparable to that used in Fig. 6(b), which explains the difference between the results shown in these figures. If the angular width α of the emission were large enough, these differences would disappear, because in such a case the peaks intensity and not their number would change when varying the NA.

4. Discussion

In order to explain the origin of the observed peaks in the RL emission, we assume that when the active material is pumped, each absorbed pump photon excites a dye molecule, which, if we do not consider amplification (stimulated emission), will emit a spontaneous emission photon. If we

Optics EXPRESS

neglect spurious absorption or auto-absorption effects, each one of these photons emitted inside the active medium as spontaneous emission will leave the active material after having traveled a distance inside it, in which it can be amplified, generating in turn new photons identical to the original. The number of new photons created depends on its gain, which is given by the population inversion density and the length of the concrete path done by the photon. Unlike other models [18,27,31–33,40] we do not care about needed resonators or feedback, only about the distribution of photon paths and their amplification.

When each pack of amplified spontaneous emission (ASE) photons leaves the surface at SSDRL, it will do with a given linear momentum and energy, or what is the same, at one concrete wavelength and direction, with a frequency-time uncertainty $\Delta\omega\cdot\Delta t\cong 1$, as has been experimentally found. Each pack of photons will be thus emitted in a random wavelength (bounded by the gain band) and direction.

To get an idea of the number of photons involved in the measurement, let us consider the particular case of Figs. 2(c) and 3(c), where the pump energy is 20 μJ, well below threshold (about 40 μJ under these pumping conditions), that we will use as a reference. If we take into account the reflected pumping (about 50%), we estimate a total possible emission of 3×10^{13} photons throughout the spontaneous emission time (about 10 ns), and of the order of 10^9 photons each coherence time (about 0.3 ps). If we assume coherent emission areas on the SSDRL surface of the size of the transport length (few tens of microns) we can have the order of 10^3 different coherent areas or more, so that during each coherence time about 10^6 photon packs could be emitted from each one. Though each pack comes from a certain coherent zone of the emitting surface, their number is too big and their intensity is too small to be able to discriminate them spatially, at least in a simple way.

If we now take into account the numerical aperture of the L1 lens, a Lambertian emission and the ratio between sizes of the measurement area and SSDRL total emission area, the ratio of photons that can enter the measurement system respect to the total emitted is of the order of 10^{-5}. Therefore, for a pumping energy of 20 μJ, the total number of photons that can be detected is about 3×10^8 and about 10^4 in a time of the order of the coherence time. Note that we are talking about photons that can be emitted spontaneously, although a variable proportion of them may be emitted as stimulated emission.

Above threshold, in addition to having more emitted photons, the vast majority of them are stimulated in the narrow time frame (tens of ps) in which the laser emission "itself" occurs. A great number of spontaneous photons will be strong enough amplified and we will have emissions at many wavelengths and directions, saturating the emission of the SSDRL, as can be seen in Figs. 2(a) and 3(a) for example. If the threshold is not reached, or long after the pump pulse, when population inversion falls below the threshold value, the probability of emission of strong peaks is much lower, and depending on the remaining level of population inversion, the system may emit more or fewer photon packs, always at random wavelengths and directions, within the spectro-temporal range of spontaneous emission. In this conditions, at a given instant, it is very likely that almost nothing besides spontaneous emission and/or noise could be observed.

An estimate of the number of spectro-temporal peaks observed can be attempted. If we consider, as expected, an exponential path-length distribution [41–43], the number of photons of spontaneous emission that follow a path of effective length longer than a given l is

$$n(>l) = n_0 \exp(-l/l_0), \tag{2}$$

where l_0 is the mean path length done by them, and n_0 is the total number of spontaneous photons considered. For a 20 μJ pumped pulse n_0 is in the order of 10^4 in a coherence time, and 3×10^8 in all the emission time if we are talking about of detected packs. On the other hand, we must bear in mind that each spontaneous emission photon, in the amplifying medium, will output a number

Optics EXPRESS

of photons equal to

$$G = \exp(\sigma N l), \tag{3}$$

where N is the average population inversion density and σ the stimulated emission cross-section. Combining expressions (2) and (3) we obtain expression (4) for the number of photon packs of gain greater than G, that enter the measurement system

$$\text{Ln } n(>G) = \text{Ln } n_0 - \frac{\text{Ln } G}{\sigma N l_0}. \tag{4}$$

On the other hand, we need a criterion that could be phenomenological, to define when any intensity fluctuation can be considered an observable peak. For that purpose, we have compared the total number of photons that could be detected under 20 μJ pump energy (3×10^8) and the total number of counts measured in averaged records under the same conditions. As a result, we have estimated that the number of photons per count is in the order of 100. Based on this observation, and taking into account that about ten counts are necessary to differentiate it from noise, we have concluded that about 1000 photons are thus required and we have established Ln $G = 7$ as a minimum limit to consider it as a peak and not as noise.

Equation (4) is applied in Fig. 8 for different cases and it explains the observed behavior, almost even quantitatively, in a simple way. Figure 8(a) shows the result corresponding to a pulse like that of Fig. 2(a) (100μJ pumping, 2mm diameter, far above-threshold), in which $\sigma N l_0 \approx 1$ is fulfilled. In this case, although the pumping is higher (×5), Ln (n_0) is incremented in only one unit, due to saturation of the population inversion density above threshold; as a result the logarithm of the number of ASE photon packs that could be registered is Ln $n(>\text{Ln}G = 7) \approx 3$, which corresponds to about 20 peaks each coherence time. This result can be compared with the number of peaks observed in either of the two spectra shown in Fig. 5(b), measured under the same pumping energy, obtaining a good agreement. Take into account that in these spectra a single pixel line is collected, which in time is approximately equivalent to that of coherence.

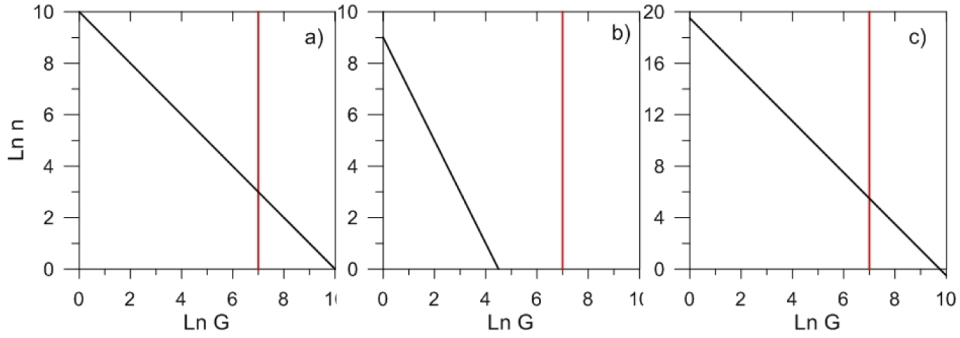

Fig. 8. Ln n of gain greater than a given G versus Ln G. The intersection between this line and the vertical Ln $G = 7$ gives us the logarithm of the number of peaks detected. a) 100μJ pump energy and diameter of the beam size 2 mm (above-threshold, $\sigma N l_0 \approx 1$). Detection time is about the coherence time (0.3 ps). b) 20μJ pump energy and diameter of the beam size 2 mm. Below-threshold ($\sigma N l_0 \approx 0.5$). Detection time is about the coherence time (0.3 ps). c) The same as (b), but with a detection time of 10 ns.

A second case is presented in Fig. 8(b), where we consider again the pumping of 20 μJ, below threshold, and therefore a minor population inversion density, for example $\sigma N l_0 = 0.5$. Figure 8(b) shows that Ln $n(>\text{Ln}G = 7) < 0$, which means that the detection of a peak (in a time equal to the coherence time) becomes a possible but infrequent event, which compares well with what is seen in Fig. 2(c), for a pulse obtained under the same conditions.

Optics EXPRESS

Finally, in Fig. 8(c) the analysis is made under the same pumping conditions than Fig. 8(b) but regarding all the detected photons (about 3×10^8 photons). In this case the result is Ln n (>Ln $G = 7$) ≈ 5, that is, of the order of 100 photon packs detected, which compares well with what is seen in Fig. 3(c) for a pulse under the same conditions.

In summary, we have showed that the spectral and temporal properties of the emission of SSDRLs can be satisfactorily explained regarding the dependence of amplification on the path length done by single spontaneous emission photons.

Funding. Eusko Jaurlaritza (PIBA 2018-24); Ministerio de Economía y Competitividad (MINECO MAT2017-87035-C2-2_P, MINECO PID 2020-115419GB-C21/C22).

Disclosures. The authors declare no conflict of interest.

Data Availability. Data underlying the results presented in this paper are not publicly available at this time but may obtained from the authors upon reasonable request.

References

1. M. A. Noginov, Solid-State Random Lasers (Springer, 2005).
2. C. Gouedard, D. Husson, C. Sauteret, F. Auzel, and A. Migus, "Generation of spatially incoherent short pulses in laser pumped neodymium stoichiometric crystals and powders," J. Opt. Soc. Am. B **10**(12), 2358–2363 (1993).
3. B. Redding, M. A. Choma, and H. Cao, "Speckle-free laser imaging using random laser illumination," Nat. Photonics **6**(6), 355–359 (2012).
4. M. Barredo-Zuriarrain, I. Iparraguirre, J. Fernández, J. Azkargorta, and R. Balda, "Speckle-free near-infrared imaging using a Nd^{3+} random laser," Laser Phys. Lett. **14**(10), 106201 (2017).
5. A.S.L. Gomes, A.L. Moura, C.B. de Araujo, and E.P. Raposo, "Recent advances and applications of random lasers and random fiber lasers," Prog. Quantum Electron. **78**, 100343 (2021).
6. F. Luan, B. Gu, A.S.L. Gomes, K.T. Yong, S. Wen, and P.N. Prasad, "Lasing in nanocomposite random media," Nano Today **10**(2), 168–192 (2015).
7. Q. Song, S. Xiao, Z. Xu, J. Liu, X. Sun, V. Drachev, V. M. Shalaev, O. Akkus, and Y. L. Kim, "Random lasing in bone tissue," Opt. Lett. **35**(9), 1425–1427 (2010).
8. S. Kéna-Cohen, P. N. Stavrinou, D. C. Bradley, and S. A. Maier, "Random lasing in low molecular weight organic thin films," Appl. Phys. Lett. **99**(4), 041114 (2011).
9. A. Consoli, D. Mariano da Silva, N. U. Wetter, and C. López, "Large area resonant feedback random lasers based on dye-doped biopolymer films," Opt. Express **23**(23), 29954–29963 (2015).
10. F. Yao, H. Bian, Y. Pei, C. Hou, and X. Sun, "Behaviors of random laser dye-doped nematic liquid crystals," Opt. Commun. **359**, 15–19 (2016).
11. J. Azkargorta, I. Iparraguirre, M. Barredo-Zuriarrain, S. García-Revilla, R. Balda, and J. Fernández, "Random laser action in Nd:YAG crystal powder," Materials **9**(5), 369 (2016).
12. M. Sobczyk and D. Szymanski, "Luminescence properties of Nd^{3+} doped $Y_2Te_4O_{11}$ microcrystalline powder," J. Lumin. **183**, 226–232 (2017).
13. S. H. Lin, P. Y. Chen, Y. H. Li, C. H. Chen, J. H. Lin, Y. H. Chen, S. Y. Tsai, and J. J. Wu, "Manipulation of polarized random lasers from dye-doped twisted nematic liquid crystals within wedge cells," IEEE Photonics J. **9**(2), 1 (2017).
14. R. Reisfeld, "Prospects of sol-gel technology towards luminescent materials," Opt. Mater. **16**(1-2), 1–7 (2001).
15. C. Sanchez, B. Lebeau, F. Chaput, and J. P. Boilot, "Optical properties of functional hybrid organic-inorganic nanocomposites," Adv. Mater. **15**(23), 1969–1994 (2003).
16. S. Y. Lam and M. J. Damzen, "Characterization of solid-state dyes and their use as tunable laser amplifiers," Appl. Phys. B **77**(6-7), 577–584 (2003).
17. O. García, L. Garrido, R. Sastre, A. Costela, and I. García-Moreno, "Synthetic strategies for hybrid materials to improve properties for optoelectronic applications," Adv. Funct. Mater. **18**(14), 2017–2025 (2008).
18. I. Iparraguirre, J. Azkargorta, S. García-Revilla, J. Fernández, and R. Balda, "Input/output energy in solid state dye random lasers," Opt. Express **27**(14), 19418–19425 (2019).
19. A. Tulek, R.C. Polson, and Z.V. Vardeny, "Naturally occurring resonators in random lasing of π-conjugated polymer films," Nat. Photonics **6**, 303–310 (2010).
20. J. Fallert, R.J.B. Dietz, J. Sartor, D. Schneider, C. Klingshirn, and H. Kalt, "Co-existence of strongly and weakly localized random laser modes," Nat. Photonics **3**(5), 279–282 (2009).
21. H. Cao, J.Y. Xu, S.H. Chang, and S.T. Ho, "Transition from amplified spontaneous emission to laser action in strongly scattering media," Phys. Rev. E **61**(2), 1985–1989 (2000).
22. M. Leonetti, C. Conti, and C. López, "Random laser tailored by directional stimulated emission," Phys. Rev. A **85**(4), 043841 (2012).
23. S. Mujumdar, V. Türk, R. Torre, and D.S. Wiersma, "Chaotic behavior of a random laser with static disorder," Phys. Rev. A **76**(3), 033807 (2007).
24. T. Sun, Z. R. Qiu, H.R. Su, D. Zhang, Z. Q. Zhang, G.K.L. Wong, and K.S. Wong, "Dynamics of random laser and coherent backscattering of light oz ZnO amplifying random medium," Appl. Phys. Lett. **91**(24), 241110 (2007).

Optics EXPRESS

25. A. Camposeo, M. Polo, P. del Carro, L. Silvestri, S. Tavazzi, and D. Pisignano, "Random lasing in an organic light-emitting crystal and its interplay with vertical cavity feedback," Laser Phot. Rev. **8**(5), 785–791 (2014).
26. S. Bittner, S. Knitter, S.F. Liew, and H. Cao, "Random-laser dynamics with temporally modulated pump," Phys. Rev. A **99**(1), 013812 (2019).
27. C.M. Soukoulis, X. Jiang, J.Y. Xu, and H. Cao, "Dynamic response and relaxation oscillations in random lasers," Phys. Rev. B **65**(4), 041103 (2002).
28. B. Liu, A. Yamilov, Y. Ling, J.Y Xu, and H. Cao, "Dynamic nonlinear effect on lasing in a random medium," Phys. Rev. Lett. **91**(6), 063903 (2003).
29. R.C. Polson, M.E. Raikh, and Z. V. Vardeny, "Universal properties of random lasers," IEEE Sel. Top. In Quantum Electron. **9**(1), 120–123 (2003).
30. S. García-Revilla, J. Fernández, M. Barredo-Zuriarrain, L.D. Carlos, E. Pecoraro, I. Iparraguirre, J. Azkargorta, and R. Balda, "Diffusive random laser modes under a spatiotemporal scope," Opt. Express **23**(2), 1456–1469 (2015).
31. M. Bahoura, K.J. Morris, G. Zhu, and M.A. Noginov, "Dependence of the Neodymium random laser threshold on the diameter of the pumped spot," IEEE J. Quantum Electron. **41**(5), 677–685 (2005).
32. J. Azkargorta, M. Bettinelli, I. Iparraguirre, S. García-Revilla, R. Balda, and J. Fernández, "Random Lasing in Nd:$LuVO_4$ crystal powder," Opt. Express **19**(20), 19591–19599 (2011).
33. M.A. Noginov, N.E Noginova, H.J. Caulfield, P. Venkatesvarlu, T. Thompson, M. Mahdi, and V. Ostroumov, "Shortpulsed stimulated emission in the powders of $NdAl_3(BO_3)_4$, $NdSc_3(BO_3)_4$, and Nd:$Sr_5(PO_4)_3F$ laser crystals," J. Opt. Soc. Am. B **13**(9), 2024–2033 (1996).
34. K.L van der Molen, A.P. Mosk, and A. Lagendik, "Relaxation oscillations in long-pulsed random lasers," Phys. Rev. A **80**(5), 055803 (2009).
35. R. Diaz, R. Courchinoux, J. Luce, C. Rouyer, J. L. Rullier, and J. Y. Natoli, "Experimental evidence of temporal and spatial incoherences of Q-Switched Nd:YAG nanosecond laser pulses," Appl. Phys. B **121**(4), 439–451 (2015).
36. I. Iparraguirre, J. Azkargorta, J. Fernández, R. Balda, S. García-Revilla, and N. Hakmeh, "On the temporal behavior of Nd^{3+} random lasers," Opt. Lett. **38**(18), 3646–3649 (2013).
37. Unpublished results of our group.
38. M.A. Illarramendi, I. Aramburu, J. Fernández, R. Balda, S.N. Williams, J.A. Adegoke, and M.A. Noginov, "Characterization of light scattering in translucent ceramics," J. Opt. Soc. Am. B **24**(1), 43–47 (2007).
39. I. Iparraguirre, J. Azkargorta, J. Fernández, S. García-Revilla, and R. Balda, "Energy test of an efficient random laser emission collecting system," Opt. Eng. **60**(01), 010502 (2021).
40. I. Iparraguirre, J. Azkargorta, J. Fernández, S. García-Revilla, M. Barredo-Zuriarrain, and R. Balda, "Random laser model for Nd^{3+}- doped powders and its application to stimulated emission cross-section calculations," Opt. Express **26**(23), 31018–31030 (2018).
41. S. Lepri, S. Cavalieri, G.L. Oppo, and D.S. Wiersma, "Statistical regimes of random laser fluctuations," Phys. Rev. A **75**(6), 063820 (2007).
42. E. Ignesti, F. Tommasi, L. Fini, S. Lepri, V. Radhalakshmi, D. Wiersma, and S. Cavalieri, "Experimental and theoretical investigation of statistical regimes in random laser emission," Phys. Rev. A **88**(3), 033820 (2013).
43. F. Tommasi, E. Ignesti, L. Fini, and S. Cavalieri, "Controlling directionally and the statistical regime of the random laser emission," Phys. Rev. A **91**(3), 033820 (2015).